# Ultrafast shear acoustic waves in liquids

T. Pézeril,[1,*] C. Klieber,[2] S. Andrieu,[3] and K. A. Nelson[2]

[1]*LPEC UMR CNRS 6087, Universite du Maine, Le Mans, France*
[2]*Department of Chemistry, Massachusetts Institute of Technology, Cambridge, USA*
[3]*LPM UMR CNRS 7556, Universite H. Poincare, Vandoeuvre, France*

(Received April 11, 2010)

In this article, recent progress on generation and detection of picosecond shear acoustic waves in liquids will be described. Measurements of ultrafast shear acoustic waves in glycerol and water at room temperature will be presented.

PACS numbers: 78.20.Hp, 43.35.+d, 78.40.Dw, 78.47.J

## I. INTRODUCTION

Direct experimental access to ultrafast shear structural relaxation dynamics in liquids remains challenging. On slow time scales, dynamic mechanical analysis and sonic or related measurement methods can be used. Faster responses at MHz frequencies are accessible to ultrasonics and impulsive stimulated thermal and Brillouin scattering, and the low GHz range may be accessed through spontaneous Brillouin scattering. Recent work in x-ray Brillouin scattering has accessed THz longitudinal acoustic frequencies; however, this technique is not yet capable of measurements at shear acoustic frequencies in liquids. Deep-UV Brillouin scattering from longitudinal acoustic waves in this range has been demonstrated. However, it is poorly adapted to measurements of shear relaxation in non-viscous liquids where acoustic damping is strong. Picosecond ultrasonics has provided tabletop access to most of the GHz frequency range for longitudinal acoustic waves. Adaptations of this method for GHz shear wave generation through sudden laser interaction with a peculiar sample with broken transverse isotropic symmetry have been developed in the recent years. However, studies of shear waves in liquids have remained elusive.

We will describe a novel approach for generation of frequency-tunable shear acoustic waves in the GHz frequency range. We will further demonstrate a sample and optical configuration that allows measurements on viscous and non-viscous liquids [1]. Results in the GHz frequency range for glycerol and water will be shown.

### I-1. Generation of GHz shear acoustic waves

In picosecond ultrasonics, plane longitudinal acoustic waves at GHz-THz frequencies can be generated by laser light absorption. Due to symmetry considerations and as a consequence of the isotropy of the thermoelastic generation, this generation mechanism is restricted only to the excitation of the longitudinal acoustic mode. To overcome this shortcoming, it has been demonstrated that it is required to break the transverse sample

 

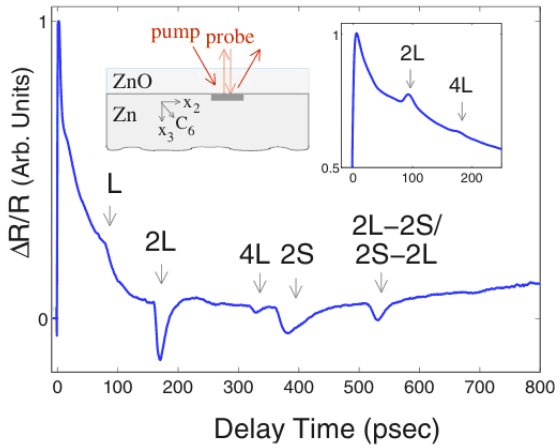


FIG. 1: Change in transient reflectivity for a Zn single-crystal substrate with tilted $C_6$ and on which a transparent ZnO film has been deposited. The break of transverse symmetry ensures the direct thermoelastic generation of plane shear waves, which are partially transmitted into the ZnO film. The shear acoustic wave packet is then detected after one round trip inside the ZnO film (labeled as 2S echo in the transient reflectivity signal). The excitation of longitudinal waves does not require such a canted symmetry. Thus, in case of a Zn single crystal whose normal surface coincides with the $C_6$ axis, only longitudinal waves are excited (as revealed by detection of the 2L and 4L longitudinal echoes shown in the inset).

symmetry. Shear acoustic wave components were generated in an off-axis oriented Zn single crystal [2–5], see Figure 1, or by use of an off-axis $TeO_2$ transparent substrate coated by an Al layer [6]. Examples employing other types of photoacoustic generation mechanisms, including electron deformation potential mechanism in GaAs/AlAs off-axis superlattices [7] as well as in 001-oriented free standing Si [8] with less than 0.2° of surface miscut (in this case the electron beam probe greatly enhances the shear detection sensitivity), and piezoelectric transduction in off-axis GaN [9], illustrate new possibilities for shear wave generation.

The general trend of breaking the transverse symmetry of the sample seems to be the most straightforward and effective way to facilitate photoacoustic shear wave generation. However, this technique is based on the so-called asynchronous shear wave generation mechanism [4, 5], which has the undesirable effect of reducing the bandwidth of the expected shear acoustic wave packet. This effect is clearly evidenced in Figure 1, where the comparison of the L-longitudinal and S-shear echo shapes illustrate the fact that the rise of the shear front is smoother than for the longitudinal front. It means that the shear strain rise, right after the laser action, experiences a delay caused by the acoustic interference of the excited quasi-mode. The excitation of the two quasi-acoustic modes, quasi-shear (QS) and quasi-longitudinal (QL) interfere with each other in the transverse direction and lead to an initially only virtual source of shear acoustic waves. Real shear waves only appear after two modes separate spatially and temporally due to their difference in propagation

speeds.

To overcome this effect and to facilitate THz shear acoustic wave generation, it will be necessary to investigate the possibility to excite shear waves in a different kind of sample or through another photoacoustic generation mechanism. For example, laser induced gratings could provide means to excite shear waves directly in an isotropic sample through ISRS [10] or through a thermoelastic process [11].

The sample used in the following experiments belongs to the category of canted transducers and therefore utilizes the so-called asynchronous mechanism of shear generation, which limits the acoustic frequency bandwidth. However, at the frequency range of interest in our experiments, this effect can probably be neglected.

### I-2. Detection of GHz shear acoustic waves

The detection of shear waves requires some particular optical configuration. Because of the particular interaction of light with shear acoustic waves, it is preferred to detect the flip of polarization of the incoming probe light [12], which is caused by shear waves only. This detection technique is sometimes referred to by the name depolarized Brillouin scattering. Depolarized Brillouin scattering detection is efficient only when the shear acoustic wave polarization is perpendicular to the optical plane of incidence. Therefore, it is important to carefully orientate the sample in the proper direction which ensures the right direction of the shear acoustic polarization. The longitudinal wave detection does not require any particular optical configuration.

## II. EXPERIMENT

In this section, we will describe an approach for generation of frequency-tunable shear as well as longitudinal acoustic waves in the GHz frequency range. We further demonstrate a sample and optical configuration which allows measurements on viscoelastic liquids. We present results from glycerol and water at room temperature, in which shear acoustic waves up to 50 GHz have been characterized. Our approach opens the door to versatile shear and longitudinal acoustic spectroscopy of bulk materials and of nanometer solid and liquid layers down to monolayer thicknesses.

In the present front-back optical pump-probe type measurement, see Figure 2(A), longitudinal and shear acoustic waves were optically generated in an iron semi-transparent thin film upon ultrafast laser irradiation. The iron films of about 50 nm thickness were obliquely deposited under ultra-high vacuum [13] with an oblique inclination angle of about 60°, which resulted in a tilt of the crystal symmetry axis of about 40°, see Figure 2(B). The canted symmetry of the iron film ensures direct generation of shear acoustic wave. Both longitudinal and shear acoustic waves may propagate into and through an adjacent layer of liquid and can be detected directly after transmission into a transparent medium through time-domain Brillouin light scattering. The strain pulses interact with the liquid which leads to spatial broadening and distortion due to frequency-dependent damping and dispersion. In the transparent substrate medium, the broadened propagating longitudinal and shear

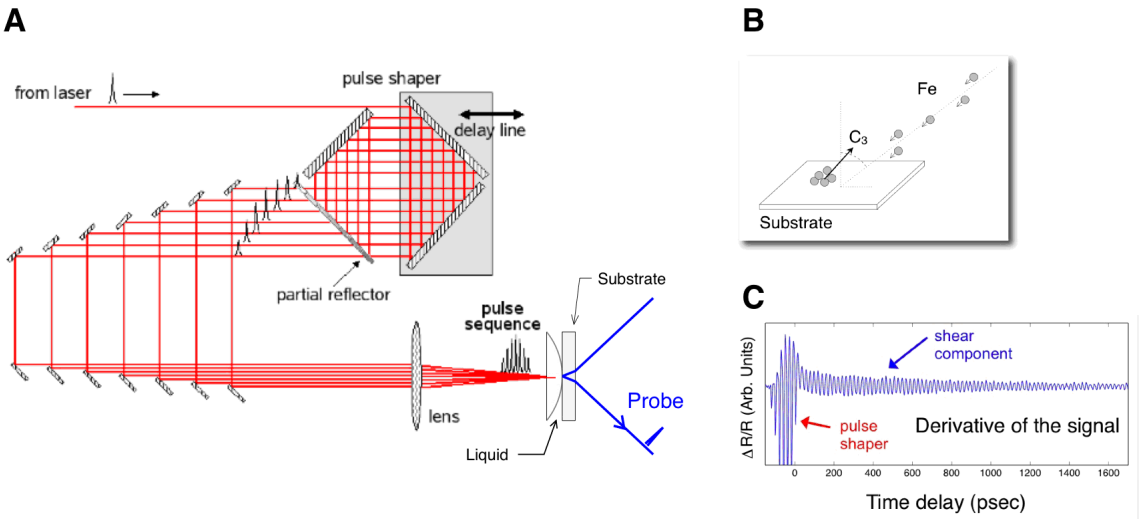


FIG. 2: (A) Schematic illustration of the optical pulse shaper of 800-nm laser wavelength. The sample cell is constructed of a liquid squeezed in between a transparent flat substrate and a plano-convex lens. The curved side of the lens is coated with an iron thin film with canted crystallographic orientation. A sequence of seven optical excitation pulses generates multiple-cycle acoustic waves in the iron film. After propagation through the liquid layer, the acoustic waves are detected in the transparent solid substrate by time-resolved coherent Brillouin scattering by variably delayed 400-nm probe pulses. (B) The iron films were deposited through MBE at oblique incidence. (C) The pulse sequence timing is adjusted to match either the longitudinal or the shear Brillouin frequency of the substrate for the optimal signal level.

strains perturb the permittivity tensor, which backscatter and flip the polarization of (only in the shear case) the incoming probe light. This effect is known as coherent (depolarized in the shear case) Brillouin scattering. In the present configuration, this phenomenon was observed in the time domain as an oscillatory signal at the so-called Brillouin frequency (see Fig. 2(C)). This frequency is determined by the probe wavelength, the angle of incidence, the refractive index, and acoustic speed in the propagating medium. Longitudinal and shear acoustic wave packets travel at different speeds, resulting in two different Brillouin frequencies. The specific interaction of propagating shear waves with light entails the back-scattered light portion to be flipped in polarization and hence allows them to be detected through depolarized Brillouin scattering at oblique incidence. Typically, the signal-to-noise levels of the recorded signals are rather poor and our approach to overcome this shortcoming is the excitation of narrowband (multiple-cycle) acoustic wave packets. This is accomplished by generating a pulse sequence with tunable frequency [14] and thus, resonantly enhancing the extremely weak shear Brillouin scattering frequency components. Combining these two techniques allows us to quantitatively analyze the interaction of high-frequency shear waves with liquids. In contrast to conventional Brillouin spectroscopy, this experimental approach makes possible the measurement not only of the amplitude but also of the phase of the Brillouin scattering which is also linked to the acoustic information of the liquid.

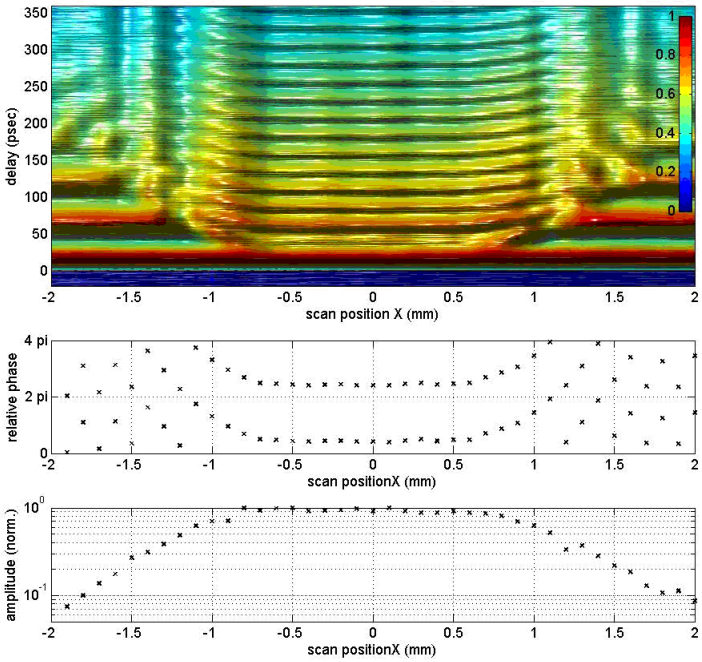


FIG. 3: (Top figure) Interpolated 2D plot of about 40 longitudinal wave data sets recorded as a function of probe delay time (plotted vertically) at different lateral (X) positions across the sample (displayed horizontally). A single excitation pulse rather than a pulse sequence was used in this case. The high-frequency signal oscillations at 40 GHz correspond to Brillouin scattering from longitudinal acoustic waves in a BK7 glass substrate, while the low-frequency oscillations at 18 GHz correspond to Brillouin scattering from the acoustic waves in liquid glycerol. Away from the center of the sample ($|X| > 0.5$ mm) the transit time through the liquid layer is apparent as a delay in the start of substrate acoustic propagation and a phase shift in the signal oscillations relative to the phase at the center of the sample. Normalized phase shifts and amplitude values of the 40-GHz high-frequency Brillouin signal oscillations from the spectrum analysis of the signal are displayed in the middle and bottom of the figure.

Theoretically, the detected probe light undergoes time-dependent intensity modulation at the Brillouin frequency $\nu$ of the gauge material, and follows $\delta I = A\cos(2\pi\nu t + \phi)$, where $A \equiv \exp(-\Gamma d)$, $\phi \equiv -2\pi\nu(d/\nu)$. Here, the Brillouin phase shift $\phi$ is proportional to the traveling time of the acoustic wave through the liquid of thickness $d$ at the acoustic speed $\nu$. The Brillouin scattering amplitude $A$ is given by the liquid sample thickness and the attenuation coefficient $\Gamma$.

Our experimental approach was comprised of a sequence of steps. We started by recording the time-resolved longitudinal Brillouin scattering at different X positions on the lens, as shown in Figure 3. The following step utilized the phase shift formula and the

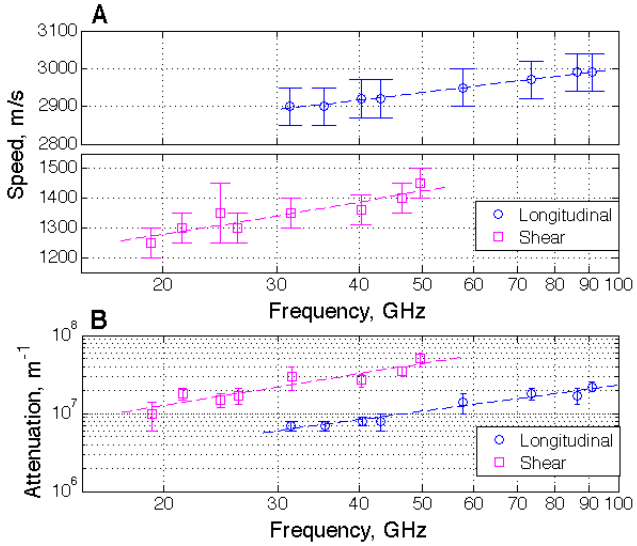


FIG. 4: Results of shear and longitudinal acoustic speeds (A) and attenuation coefficients (B) in liquid glycerol at room temperature.

known curvature of the lens to map out the liquid thickness topography. Fourier analysis of the Brillouin signal then yielded the value for the mean longitudinal speed of sound and attenuation over the whole scanned area. Subsequently, we recorded the corresponding shear Brillouin scattering data at the same X positions as for the longitudinal data by using the technique of enhanced generation and detection as described above. The shear speed of sound could then be deduced from the phase shift extracted from polarization flipped scattering measurements. The fitting parameter in this case is the shear speed of sound. Like for the analysis of the longitudinal attenuation, the shear acoustic damping coefficient $\Gamma$ was deduced from the measurement of the shear Brillouin amplitude by averaging over all calculated values of a data set at a given Brillouin frequency.

In order to obtain the longitudinal and shear speed of sound and attenuation information over a broad range of Brillouin frequencies, we repeated our measurements for each tandem Brillouin frequencies by changing the probe refraction angle inside the substrate medium by use of a prism. In addition, we conducted experiments with either sapphire or glass as a detection medium, which allowed us to access a longitudinal frequency range from 91 to 57 GHz with sapphire and 43 to 31 GHz with glass, and a shear frequency range from 50 to 31 GHz with sapphire and 26 to 19 GHz with glass. Figure 4 shows the results of the acoustic speed and attenuation measurements of glycerol.

Measurements on water are currently under way and are slightly different than those on glycerol. This is mainly because of the strong attenuation of shear waves in water in comparison with glycerol. Therefore, it was not possible to reliably assume the liquid topography from the lens curvature for thicknesses down to a couple of nanometers. To overcome this, we used literature values for the longitudinal speed of sound in water. The

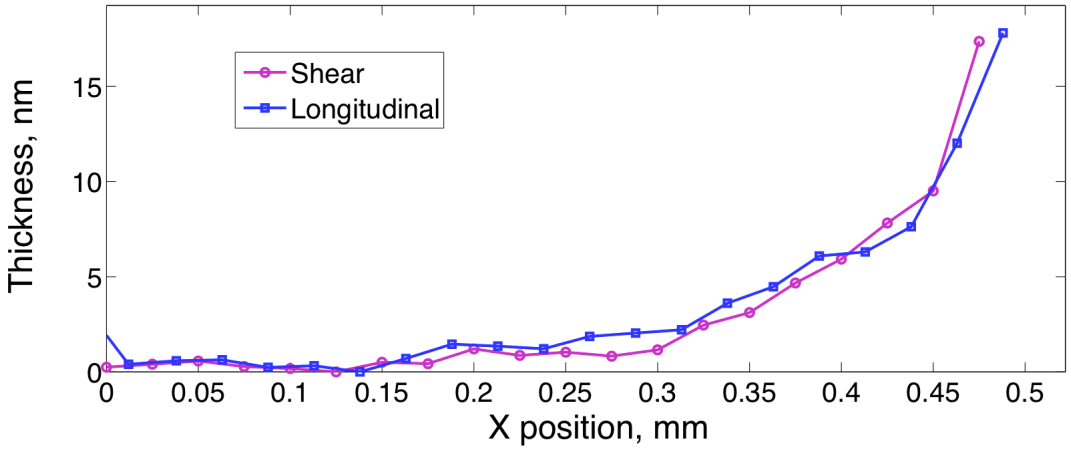


FIG. 5: Topography of a water layer at room temperature calculated from Brillouin scattering measurements at 42 GHz (longitudinal) and 25 GHz (shear).

required liquid topography was then deduced from the analysis of the Brillouin longitudinal phase shift, assuming the value for the longitudinal speed of sound of 1500 m/s from the reference [15]. The analysis of the amplitude of longitudinal Brillouin scattering enabled the determination of the longitudinal damping value of $\Gamma_L = 35 \cdot 10^6$ m$^{-1}$. From the shear depolarized Brillouin scattering measurements, conducted at similar lateral positions X and the use of the above described technique of enhanced Brillouin detection, we were able to detect shear Brillouin component of shear waves that propagate in water at 25 GHz. Our experiment will help to better understand shear relaxation mechanisms in water. Moreover, by fitting the shear speed of sound that best matches the longitudinal and the shear topography, see Fig. 5, we determined the value of the shear speed of sound in water to $\nu_s = 660$ m/s. Subsequently, from the analysis of the shear Brillouin amplitude, we got a value for the attenuation of $\Gamma_s = 120 \cdot 10^6$ m$^{-1}$, which was one order of magnitude higher than that for glycerol at the same frequency. This allows to calculate the dynamic viscosity $\eta$ of water at 25 GHz by the fundamental equation [16] $\eta = \Gamma_s \rho \nu_s^3/(2\pi\nu)^2 = 1.4 \cdot 10^{-3}$ Pa-s and yields a value close to the static viscosity of $1 \cdot 10^{-3}$ Pa-s. This can be interpreted such that there is very little shear relaxation present in this frequency range. The ratio of the shear wavevector to the attenuation coefficient gives a value of $2\pi\nu_s/\nu_s\Gamma_s \sim 2 > 1$, telling that the shear wave at this frequency is purely viscoelastic rather than diffusive. This means that the shear threshold frequency of propagation is even lower than 24 GHz.

## III. CONCLUSIONS

Recent progress on the generation and detection of picosecond shear acoustic waves in different media, described in the present article, has reached the point where measurements

of shear waves propagating in liquids have become possible. The key to this challenging problem has been the continuous effort on the implementation of shear photoacoustic transducers with higher and higher efficiency at GHz frequencies. We believe that in the next decade, new types of samples will reach THz frequencies for shear waves in a similar way as already possible in the case for longitudinal waves. Ultimately, photoacoustic experiments will be able to cover the frequency range from MHz to THz at both longitudinal and shear polarizations.

**Acknowledgments**

This work was partially supported by CNRS, the Department of Energy Grant No. DE-FG02-00ER15087 and National Science Foundation Grants No. CHE-0616939 and DMR-0414895. The authors would like to thank Vitaly Gusev for the fruitful discussions and comments.

## References

* Electronic address: thomas.pezeril@univ-lemans.fr

[1] T. Pezeril, C. Klieber, S. Andrieu, K. A. Nelson, Phys. Rev. Lett. **102**, 107402 (2009).
[2] D. H. Hurley, O. B. Wright, O. Matsuda, V. E. Gusev, O. V. Kolosov, Ultrasonics **38**, 470 (2000).
[3] O. Matsuda, O. B. Wright, D. H. Hurley, V. E. Gusev, K. Shimizu, Phys. Rev. Lett. **93**, 095501 (2004).
[4] T. Pezeril, N. Chigarev, P. Ruello, S. Gougeon, D. Mounier, J.-M. Breteau, P. Picart, V. Gusev, Phys. Rev. B **73**, 132301 (2006).
[5] T. Pezeril, P. Ruello, S. Gougeon, N. Chigarev, D. Mounier, J.-M. Breteau, P. Picart, V. Gusev, Phys. Rev. B **75**, 174307 (2007).
[6] T. Bienville and B. Perrin, Proc. WCU, **813** (2003), sfa.asso.fr/wcu2003/procs/website/.
[7] P. Walker, R. P. Campion, A. J. Kent, D. Lehmann, Cz. Jasiukiewicz, Phys. Rev. B **78**, 233307 (2008).
[8] M. Harb, W. Peng, G. Sciaini, C. T. Hebeisen, R. Ernstorfer, M. A. Eriksson, M. G. Lagally, S. G. Kruglik, R. J. D. Miller, Phys. Rev. B **79**, 094301 (2009).
[9] Y.-C. Wen, T.-S. Ko, T.-C. Lu, H.-C. Kuo, J.-I. Chyi, C.-K. Sun, Phys. Rev. B **80**, 195201 (2009).
[10] K. A. Nelson, J. Appl. Phys. **53**, 6060 (1982).
[11] V. Gusev, Appl. Phys. Lett. **94**, 164105 (2009).
[12] D. Mounier, P. Picart, P. Babilotte, P. Ruello, J.-M. Breteau, T. Pezeril, G. Vaudel, M. Kouyate, V. Gusev, Opt. Exp. **18**, 6767 (2010).
[13] P. Fréchard, S. Andrieu, D. Chateigner, M. Hallouis, P. Germi, M. Pernet, Thin Solid Films **263**, 42 (1995).
[14] J. D. Choi, T. Feurer, M. Yamaguchi, B. Paxton, K. A. Nelson, Appl. Phys. Lett. **87**, 081907 (2005).
[15] L. J. Shelton, F. Yang, W. K. Ford, and H. J. Maris, Phys. Status Solidi B **242**, 1379 (2005).
[16] K. F. Herzfeld, T. A. Litovitz, *Absorption and Dispersion of Ultrasonic Waves*, Academic press, New York and London (1959).